Local structures of copper-doped ZnO films

Qing Ma,[1,*] D. Bruce Buchholz,[2] and Robert P. H. Chang[2]
[1]*DND-CAT, Synchrotron Research Center, Northwestern University, 9700 South Cass Avenue, Argonne, Illinois 60439, USA*
[2]*Department of Material Science and Engineering, Materials Research Center, Northwestern University, Evanston, Illinois 60208, USA*

(Received 7 July 2008; revised manuscript received 20 October 2008; published 29 December 2008)

We report the local structures of a series of copper-doped zinc oxide films using polarization-dependent x-ray-absorption spectroscopy. The films were grown by pulsed-laser ablation under various conditions. The results show that films where copper exists solely as clusters are not ferromagnetic. The results also show that some of the copper-doped zinc oxide films are not ferromagnetic despite the fact that the copper substitution for zinc in the ZnO lattice is in the Cu^{2+} state, which provides the necessary unpaired spins for ferromagnetism. Therefore, Cu^{2+}/Zn^{2+} substitution is not the only imperative condition for ferromagnetism to occur. We present characteristics unique to the electronic and atomic structure of ferromagnetic films and argue that the increased covalence of the Cu_{Zn}-O bond found in these films is a prerequisite for the spin alignments in a substitutionally copper-doped zinc oxide film.

DOI: 10.1103/PhysRevB.78.214429 PACS number(s): 75.50.Dd, 78.70.Dm, 61.05.cj, 75.70.−i

I. INTRODUCTION

Thin films of copper-doped zinc oxide (ZnO:Cu) has been observed to be ferromagnetic with a transition temperature (T_C) above room temperature.[1–5] As a ferromagnetic semiconducting material, ZnO:Cu belongs to the general class of diluted magnetic semiconductors (DMSs). Among the DMS materials, Cd(Mn)Te was one of the earliest,[6] and Ga(Mn)As is a material[7] upon which much foundation research has been made. These materials, however, have a T_C below room temperature. ZnO:Cu, because it has a T_C above room temperature, is a material of promise for spintronic applications. Most DMS materials are formed by substituting magnetic ions onto lattice sites of a host material.[6] Typical materials systems include GaN doped with Mn, Cr, Ni, or Fe (Refs. 8 and 9) and ZnO doped with Mn, Co, Cr, Ni, V, or Fe.[10] A drawback to this approach is that the dopant material can segregate to form precipitates or clusters that are actually responsible for the ferromagnetic properties. The effect of such ferromagnetic clusters must be examined more carefully before the usefulness of such materials for spintronics applications can be determined.[11] ZnO:Cu has the possibility of being an unambiguous DMS; metallic zinc, ZnO, metallic copper, Cu_2O, and bulk CuO are not ferromagnetic. Only one possible ambiguity to the DMS nature of ZnO:Cu exists in that there is some indication that small CuO particles may acquire ferromagnetic order,[12] and one study of ZnO:Cu suggests that the ferromagnetic contribution to the material may originate from a planar Cu-O nanophase lying in the basal planes of the ZnO lattice.[4] This, however, was not found to be the case for our films.

The discussion as to the origin of ferromagnetism extends beyond whether it is the result of a Cu-O nanophase or not. The wide range of differing experimental observations has led to a number of hypotheses. Some studies report copper in ZnO to be in the Cu^{2+} state,[3] others the Cu^{1+} state,[2] and still others a mixed $+2/+1$ oxidation state.[1] The doping of ZnO:Cu with nitrogen has been reported both to increase the magnetic moment per Cu atom[3] and to decrease the magnetic moment per Cu atom.[2] Some studies suggest that *p*-type ZnO favors ferromagnetism[5] while other studies show that ferromagnetism can occur in materials that are clearly *n* type.[2] Even the effect of copper incorporation into ZnO on the lattice has reports of the $\hat{c}$ axis lattice constant contracting with increasing Cu concentration[1,4,5] and expanding with the incorporation of copper.[13] The only point that seems to be almost universally agreed upon is that the magnetic moment per Cu atom decreases as the Cu concentration increases although even here there is one report that at very low Cu concentration (0.5%) the magnetic moment per copper atom is observed to decrease slightly from the value at 1% copper concentration.[3] The purpose of this paper is to add our experimental observations to the body of knowledge that will enable the more informed contemplation of the mechanisms possible. We will, however, also venture our hypothesis as to how the body of experimental evidence might fit together.

II. EXPERIMENTAL ASPECTS

A series of copper-doped ZnO films was grown by pulsed-laser deposition (PLD) using a ZnO target and a Cu target. A 248 nm KrF excimer laser with a 25 ns duration and operated at 2 Hz was used. The laser beam was focused to a 1×2 mm^2 spot on the target materials. A computer-controlled shuttle was used to alternate ablation between the two targets; the number of laser pulses on each target was adjusted to obtain the desired Cu doping levels. Less than one monolayer of film was deposited in a typical ZnO-Cu cycle to help ensure a uniform distribution of Cu in the ZnO film. The films were grown on $\hat{c}$-plane sapphire substrates to a thickness of ~200 to ~300 nm with a $\hat{c}$ axis preferred orientation. The Cu content of the films was determined by inductively couple-plasma atomic-emission spectroscopy. The Cu-doped ZnO films do not have sufficient conductivity to measure electrical parameters by Hall measurement. The target-substrate (t-s) separation was fixed at 10 and 8 cm, respectively, for two sets of the films prepared in a N_2O ambient, and at 8 cm for a set of films prepared in an O_2

ambient. A superconducting quantum interference device (SQUID) magnetometer was used to measure the magnetic properties of the films between 10 and 390 K. The measurements indicate that only the films prepared at (t-s) 8 cm in a N_2O ambient are ferromagnetic. The 1% Cu shows a clear indication of a Curie temperature (T_C) around 390 K. The other films, with >1% Cu, had a Curie temperature above 390 K, the limit of the SQUID (see Ref. 5 for more details).

X-ray-absorption spectroscopy measurements were carried out at the 5BM-D bending magnet beamline of the DND-CAT located at Sector 5 of the Advanced Photon Source (APS), Argonne National Laboratory. A Si(111) monochromator is used to select the x-ray energies. A pair of the Rh-coated mirrors is employed before and after the monochromator. The first mirror collimates vertically the incoming synchrotron radiation, and the second one focuses the monochromatized beam vertically down to 0.2 mm at the full width at half maximum (FWHM) at the sample 25 m away. The incident beam size is defined by two pairs of Huber slits. The x-ray-absorption spectra around the Cu K edge were measured with the radiation polarization vector ε quasiparallel ($\parallel$) and quasiperpendicular ($\perp$) to the sample surface, respectively, for which a grazing incident angle of $2°-5°$ is used. The Zn K edge data were measured only in the $\perp\varepsilon$ geometry. The Cu $K\alpha$ and Zn $K\alpha$ emission intensities were recorded by a 13-element Ge detector at 90° to the x-ray beam path. The x-ray pulses were processed with a 1 μs peaking time using the electronics from X-ray Instrument Associate (XIA). The fluorescence intensity is corrected for the detector dead time. The incident-beam intensity was monitored by an Oxford-Danfysik ion chamber. A reference metal foil of either copper or zinc was inserted in between the second and third such ion chambers along the beam path whose absorption spectrum is measured simultaneously for energy calibration. Each sample is oriented in a way to avoid the Bragg conditions as much as possible. Self-absorption effect is verified to be largely absent in the $\parallel\varepsilon$-measured spectra.

The absorption data were processed using the ATHENA software package. The data contained only a few small well-localized Bragg peaks, from the substrate, which were easily removed. The FEFF simulations were performed wherever necessary.

III. BACKGROUND

In an x-ray-absorption process, the initial-state core electron (ψ_i) is excited into a final state (ψ_f). For a 1s core electron, the intensity of such a transition is determined by the cross section,[14]

$$\mu(\hbar\omega,\varepsilon,k) = \delta(E_f - E_i - \hbar\omega)\left(|\langle\psi_f|\varepsilon\cdot\hat{r}|\psi_i\rangle|^2 + \frac{1}{4}|\langle\psi_f|\varepsilon\cdot\hat{r},\varepsilon\cdot k|\psi_i\rangle|^2\right),$$

where $\hbar\omega$ is the photon energy, ε is the polarization vector, $\hat{r}$ is the unit vector along the interaction length R, and k is the photoelectron momentum. The first and second terms are the dipole and quadrupole contributions, respectively. For the K absorption edge of copper, the dipole transition involves $1s\rightarrow 4p$. The quadrupole transition $1s\rightarrow 3d$ is also nonzero if an inversion symmetry is lifted either vibrationally or structurally, such as the case for the $3d^9$ Cu^{2+} ion. By sweeping the x-ray energy across the absorption edge, the excited electrons will probe all the selection-rule-allowed empty states in the band structure, which gives x-ray absorption near edge structure (XANES).

With further increase in x-ray energy, the outgoing energetic electrons will be scattered by neighboring atoms. The interference between the outgoing and backscattered electrons produces sinusoidal oscillations in $\mu(\hbar\omega,\varepsilon,k)$ which can be parametrized for dipole transition:[15]

$$\chi(k) = \sum_i \frac{N_i(\theta)|f_i(k)|S_0^2}{kR_i^2}\sin[2R_ik + 2\delta_c(k) + \varphi(k)] \times e^{-2R_i/\lambda(k)}e^{-2\sigma_i^2k^2},$$

where $\chi(k)=(\mu-\mu_0)/\mu$, in which μ_0 is the atomic absorption. $\chi(k)$ contains the extended x-ray-absorption fine structure (EXAFS), of which the Fourier transform reveals the local structure around the absorbing atom, called here as the *pseudo*-radial distribution function (p-RDF), since it bears similarity to the atomic radial distribution function. f_i is the backscattering amplitude, S_0^2 is the amplitude reduction due to many-body effect,[16] and $2\delta_c$ and φ are the phase changes in the electron wave due to the central and neighboring atom potentials, respectively. The term $e^{-2R/\lambda(k)}$ is the photoelectron mean-free-path $\lambda(k)$ effect. The term $e^{-2\sigma^2k^2}$ is the Debye-Waller factor for vibrational and structural disorders in which σ is the root-mean-square fluctuation in R. By using the reference materials, bulk CuO, Cu_2O, and ZnO, and assuming chemical transferability, the λ and S_0^2 terms are presumably known. $N_i(\theta)=\Sigma_j^N 3|\varepsilon\cdot\hat{r}_j|^2$ is the projected coordination number, where θ is the angle between the directions of the polarization and the interaction.

A simple analytical method,[17] which can be derived from the EXAFS equation, is used to estimate the difference ΔR in distance for two same atomic pairs, especially when visually indistinguishable in the p-RDFs. Such interaction leaves a kink in $2\delta_c^2+\varphi$ vs k. Its position k_p is related to $\Delta R=\pi/2k_p$. Its existence thus indicates a ΔR difference. In addition, the anharmonic interaction may exist in the interatomic potential, which may be accounted for an extra term in the EXAFS phase, i.e., $2/3C_3k^3$.[18] C_3 is the EXAFS third cumulant, and its effect on the bond-length determination will be considered versus the reference materials. In this analysis the 20% Hanning window function, $\Delta R=1$ Å, and $k=2.6-10.6$ $Å^{-1}$ are used.[18]

The ZnO:Cu films have a wurtzite structure with the $\hat{c}$-plane perpendicular to the sample surface, as verified by x-ray diffraction. The films show a contraction in the $\hat{c}$-axis lattice constant with increase in the copper doping concentration. The wurtzite structure is favored by more ionic compounds. The structure (hcp) of ZnO is composed of alternating O^{2-} and Zn^{2+} planes stacked along the $\hat{c}$-axis direction,

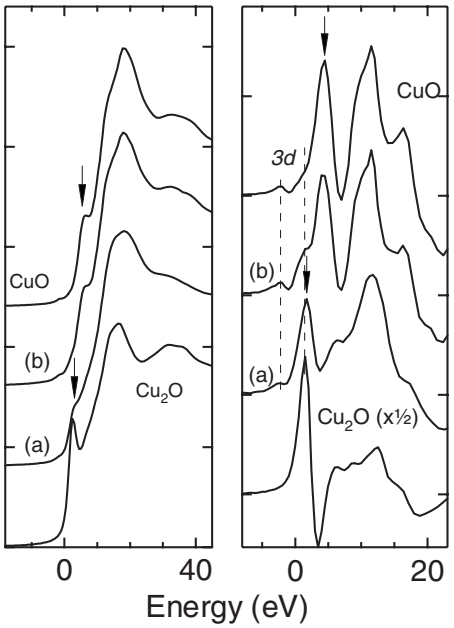

FIG. 1. Cu K edge XANES spectra (left) and the first derivatives (right) of two N_2O-prepared films and of bulk CuO and Cu_2O. The films were prepared at 10 cm target-to-substrate distance: (a) Cu 1% and (b) Cu 6%. The arrows indicate the shakedown features due to the ligand-metal charge transfer (see the main text for details). The zero energy is set to the Cu K edge of metal.

both ions being tedrahedrally coordinated. The oppositely charged atomic planes result in an electric dipole moment along the $\hat{c}$-axis direction.

IV. COPPER CLUSTERS IN THE Cu-DOPED ZnO SYSTEMS

When films are grown with 10 cm t-s in a N_2O ambient, copper oxides form clusters. Figure 1 shows the XANES spectra and their derivatives for two films with different Cu doping level, as well as reference bulk CuO and Cu_2O spectra. The sample spectra were all collected in the $\|\varepsilon$ geometry. The spectra are referenced to the Cu K edge of copper metal. A pre-edge feature located near −2 eV exists for all the spectra except for Cu_2O, better seen by the first derivatives in the right panel of Fig. 1. This feature is due to the quadrupole $1s \rightarrow 3d$ transition which is only allowed when the empty d states are available such as in the $3d^9$ electronic configuration of the Cu^{2+} ion and the structural unit around the absorbing atoms lacks centrosymmetry. The $3d^{10}$ electronic configuration of the Cu^{1+} ion prohibits such a transition. Clearly a Cu^{2+} component exists in both samples, and the 6% Cu doping sample may consist essentially of the CuO entities since its spectrum is very similar to that of CuO.

The rising edge of the 1% sample coincides roughly with that of bulk Cu_2O, and it is tempting to assign it to the Cu^{1+} state. However, the large difference in the rest of the spectrum from that of bulk Cu_2O may suggest otherwise. Mixing of the spectra of CuO and Cu_2O does not reproduce the spectrum. Together with the existing $3d$ peak, it is very likely that the rising edge of the Cu 1% sample is in fact the

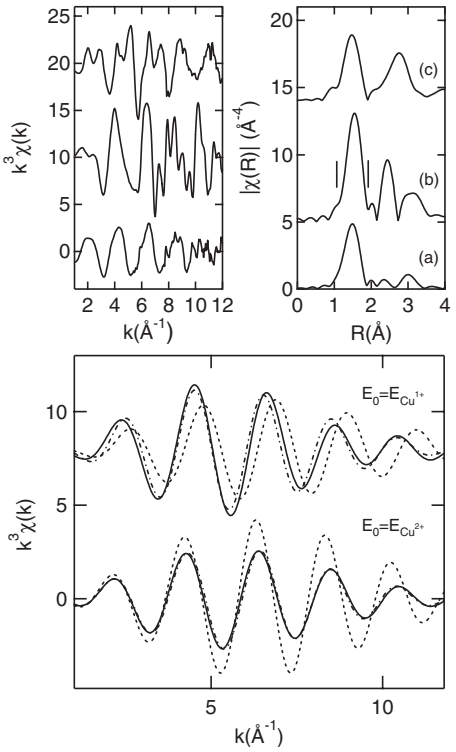

FIG. 2. Upper panel: Cu K edge EXAFS and p-RDFs of the (a) Cu-1% doped film, (b) bulk CuO, and (c) Cu_2O. Lower panel: the inverse Fourier transforms of the first peaks (within the window marked), in which the upper solid line is obtained by E_0 equal to that of Cu_2O (dashed line) and the lower solid line is obtained by E_0 equal to that of CuO (dashed line). Simulation curves (dot-dashed line) using the phases and amplitudes extracted from the Cu-O bond (dashed line) in bulk CuO and Cu_2O are also shown, respectively (barely distinguishable in the case of CuO).

"shakedown" feature of the $1s \rightarrow 4p$ transition in the Cu^{2+} ion. The shakedown feature is due to the final-state screening (or many-body effect) of the Cu $1s$ core hole by the ligand-metal charge transfer ($L \rightarrow M$) due to orbital mixing ($2p$-$3d$ mixing here).[19] It is shifted downward by 3 eV when compared with that of bulk CuO, which would suggest a stronger screening effect and possibly a larger reduction in S_0^2 as well.[16]

Figure 2, where the EXAFS and p-RDFs of the (a) 1% Cu film, (b) bulk CuO, and (c) Cu_2O are compared, is presented to further the assertion that the rising edge is a shakedown feature of the Cu^{2+} state and not of the Cu^{1+} edge. The lower panel in Fig. 2 compares the EXAFS oscillations of the Cu-O bond with those in CuO (dashed line) and Cu_2O (dashed line), in which the upper solid line represents the EXAFS of the Cu-O bond obtained for the threshold E_0 set at that of Cu_2O, while the lower solid line obtained with E_0 being equal to that of CuO. In comparison with CuO, the differences in the magnitude can be accounted for either by $N=3.3$ using the S_0^2 value of bulk CuO(=0.76) and by $e^{-2\sigma 2k2}$ ($\sigma^2=0.0075$ Å^2) or by a 17% reduction in S_0^2(=0.64) for a $[CuO_4]$ unit and by the same σ^2. The excellent fit (dot-dashed line) is seen in Fig. 2, from which $R=1.92$ Å, being 0.035 Å shorter than that in bulk CuO. However, comparison with Cu_2O is less satisfactory. A fit (dot-dashed line) is

obtained with $N=3.6$, $R=1.92$ Å, and $\sigma^2=0.006$ Å^2. The differences in the phases might be caused by the difference in the $2\delta_c$ term, which has a somewhat larger contribution to the total phase since the photoelectron experiences twice the potential of the central ion.[16] It is thus concluded that the copper ions in this sample are predominantly Cu^{2+}.

The FEFF8 simulations of the Cu-O bonds in both the film and bulk CuO with the third cumulant C_3 included give $\Delta R=0.026$, for which $C_3=(-1.7\pm0.1)\times10^{-4}$. The ΔR value remains essentially the same for the simulations without C_3 included. Therefore, this result confirms the one obtained above using the experimental phase from bulk CuO.

The shorter Cu-O distance indicates a more covalent bond, which is consistent with *increased* screening, resulting in the downward shifts of the shakedown feature.[19] Using the Brown-Shannon empirical equation for the bond covalence f,[20] it is possible to appreciate the change in bonding orbital overlapping due to the change in bond length. Here $f=as^M$, where $s=s_0(R/R_0)^{-N}$, the bond strength in valence unit; $a=0.49$, $M=1.57$, and $N=5.4$ for CuO, which are all empirical constants. The relative change in covalence may thus be calculated by $\beta=(f-f_{\text{bulk}})/f_{\text{bulk}}=(R/R_{\text{bulk}})^{-MN}-1$. For $R_{\text{CuO}}=1.955$ Å, $\beta=0.12-0.16$, a 12–16 % increase in covalence. The Cu^{2+} ions are likely in small clusters in the Cu 1% sample, say $[CuO_m]_n$ ($m\leq4$), consistent with the short Cu-O bonds and the lack of the interaction beyond the first coordination. In contrast, CuO in the Cu 6% sample are likely in a form of larger clusters. The electronic structure is nearly identical, and the local structure (not shown) is relaxed, to that of bulk CuO.

This portion of the work has described the electronic and atomic structures of the copper clusters in the films. The electronic structure of small Cu clusters may depart significantly from that of the bulk material due to the change in the bonding property. The prominent downward shift of the shakedown feature is the result of increased covalence of the Cu-O bond. Despite the differences in the details, these films are all nonferromagnetic.

V. EFFECT OF SUBSTITUTIONAL DOPING ON THE ZnO STRUCTURE

Figure 3 shows the Zn K edge XANES spectra measured with $\perp\varepsilon$ on two samples prepared at 8 cm (t-s) and a N_2O-prepared ZnO film as well as that of powder ZnO. The XANES of the ZnO film is typical for a ĉ-axis oriented ZnO film measured in this geometry.[21] The $\|\varepsilon$ XANES of the ZnO film (not shown) is quite similar to that of powder ZnO. The arrow indicates a characteristic peak that is similar to the one appearing on the Cu K edge XANES of copper doped films, as will be shown later on, when the Cu/Zn substitution occurs. For the Cu-doped films in Fig. 3, changes in the XANES are readily observable. These changes are likely the result of Cu ions, or at least a fraction of them, occupying the Zn sites. When the copper exists as clusters in the films, as discussed in Sec. IV, the Zn K edge XANES remains the same as that of the ZnO film. Thus, the clusters have a minimum effect on the band structure of the ZnO host.

Figure 4 shows the p-RDFs of the samples (lower), together with the FEFF8 simulations, and a few of the EXAFS spectra as examples (upper). The dashed frame in the EXAFS panel is used to draw attention to the enclosed oscillations which are characteristic of the ZnO structure.

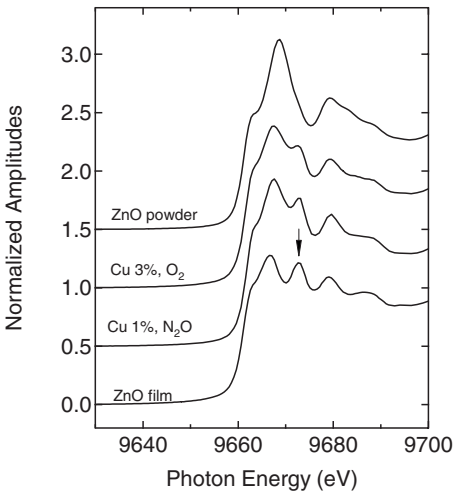

FIG. 3. Zn K edge XANES spectra of the copper-doped films prepared at 8 cm (t-s) and a ZnO film measured at $\perp\varepsilon$ compared with those of a nano-ZnO powder. The arrow indicates a characteristic peak of the ĉ-axis oriented ZnO film.

The Zn-O bond appears to be shorter for the O_2-prepared samples, while the bond lengths for the N_2O-prepared samples are similar to that for nano-ZnO. Based on the

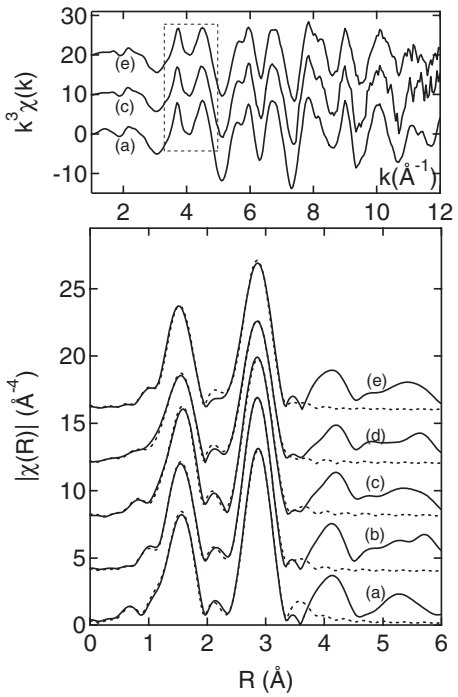

FIG. 4. Zn K edge EXAFS spectra (upper) and p-RDFs (lower) of (a) nano-ZnO; [(b) and (c)] N_2O-prepared Cu 1% and Cu 7%-doped films; [(d) and (e)] O_2-prepared Cu 3% and Cu 7%-doped films. The dashed box encloses a feature that is characteristic of the ZnO structure. The FEFF8 simulations based on (a) are also shown in lower panel (dashed lines). The k range used in the Fourier transforms is 2.6–10.6 Å^{-1}.

wurtzite structure ($S_0^2=0.9$), the FEFF8 simulations without C_3 included show that the Zn-O bond lengths in nano-ZnO and N_2O-prepared films are equal to 1.97 Å, while it is 1.96 Å for O_2-prepared films. However, the results obtained with C_3 included show that the Zn-O bond lengths for nano-ZnO and N_2O-prepared films are equal to ~1.95 Å ($C_3=-3.5\times10^{-4}$ to -4.6×10^{-4}), while it is 1.94 and 1.97 Å for O_2-prepared Cu 3% and 7% films ($C_3=-4.9\times10^{-4}$ and 1.8×10^{-4}), respectively. Therefore, the first peak for O_2-prepared Cu 7% film has different distribution ($C_3>0$) from others.[18] It is remarkable that these exercises have little effect on the σ^2 values. The local structures of O_2-prepared films, for which $\sigma^2=0.0044-0.0060$ Å^2, are considerably more disordered than those of N_2O-prepared films and nano-ZnO, for which $\sigma^2=0.0025-0.0037$ Å^2. Like nano-ZnO, the N_2O-prepared films have a kink near 9.8 Å^{-1} in the phases $[2\delta_c(k)+\varphi(k)]$ of the Zn-O interactions, indicating a splitting under the first peak by $\Delta R\sim0.16$ Å ($=\pi/2k$). This is consistent with the wurtzite structure which has three O atoms at 2.042 Å and one O atom at 1.796 Å. In fact, the negative C_3 values are likely due to such a discrete bond-length distribution; the C_3 term is sensitive to the variation in the phase at high k region since it varies with k^3.

From the simulation, $N_1(\theta)=3.4$ for N_2O-prepared films and is 3.7 for O_2-prepared films. For a wurtzite $[ZnO_4]$ unit $N_1(\theta)$ is 3.54 calculated along the $\hat{c}$-axis and $\theta=\arcsin[R_{O\text{-}O}/(\sqrt{3}R_{Zn\text{-}O})]$ ($R_{Zn\text{-}O}=2.04$ Å and $R_{O\text{-}O}=3.2$ Å). Within the accuracy of this technique, the result strongly indicates that there exist no detectable oxygen vacancies in the ZnO:Cu films.

VI. ATOMIC AND ELECTRONIC STRUCTURES OF THE Zn-SITE COPPER

From analyses of the Zn K edge absorption data, the doping effect on the local structures around the Zn atoms is described. In contrast to the cases where cluster formation is observed, substitution of Cu on Zn sites (which will be noted as Cu_{Zn}) perturbs the band structure of the films prepared in either the O_2 or N_2O environments. In the following the Cu K edge data will be presented separately for O_2 and N_2O films which are all prepared at the 8 cm (t-s) distance.

A. Cu K edge data of the O_2-prepared films

Figure 5 displays the Cu K edge XANES spectra and their first derivatives for the O_2-prepared films, measured in both $\|\varepsilon$ and $\perp\varepsilon$. For comparison, the data of bulk CuO are also presented. Weak polarization dependence is seen in the spectra which, however, do not deviate drastically from that of bulk CuO, especially the position of the $L\rightarrow M$ feature. The $3d$ peaks locate at 1 eV below that of bulk CuO. The energy difference $\Delta E_{(L\text{-}M)\text{-}3d}$ between the $3d$ and $L\rightarrow M$ features is 7.5 eV. The shoulder at ~21 eV in the $\perp\varepsilon$ data corresponds well to that observed on the Zn K edge spectra (Fig. 3) and is likely resulted from the same origin. Thus, the band structure near the doping atoms is regulated by the lattice structure. The shoulder weakens with increasing doping level; more CuO clusters form and obscure the Cu_{Zn} substitution effect.

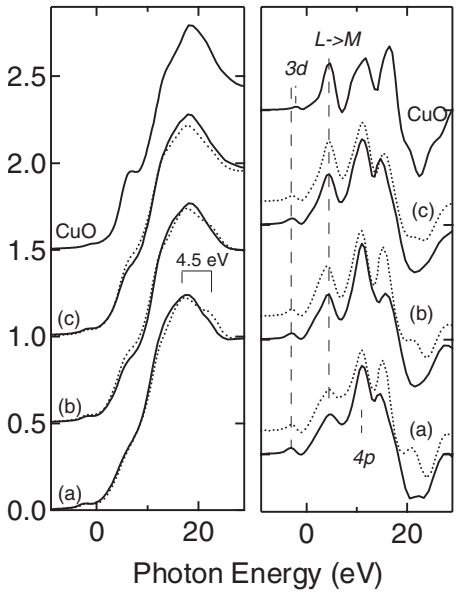

FIG. 5. Cu K edge XANES spectra and the first derivatives of O_2-prepared films measured at two sample orientations: $\|\varepsilon$ (solid line) and $\perp\varepsilon$ (dotted line). (a) Cu 3%; (b) Cu 7%; and (c) Cu 14% compared to bulk CuO. The zero energy is set to the Cu K edge of metal.

These findings are corroborated well by the changes in the EXAFS spectra. Figure 6 shows the $\perp\varepsilon$ Cu K edge EXAFS spectra (upper) and the p-RDFs (lower). The dashed frame, again, is used to emphasize the oscillation characteristic of the ZnO structure, similar to those presented in the same way in Fig. 4, suggesting readily the formation of the ZnO-like

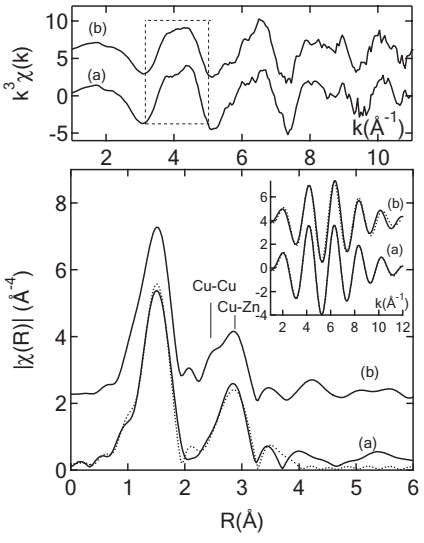

FIG. 6. Cu K edge EXAFS spectra (upper) and p-RDFs (lower) of O_2-prepared films: (a) Cu 3% and (b) Cu 7%. The dashed box encloses a feature that is characteristic of the ZnO structure (see also Fig. 4). A FEFF8 simulation of the Cu 3% film using a wurtzite $Cu_{Zn}O$ cluster is shown in the lower panel (dashed line). The insert displays the EXAFS oscillations (solid line) of the Cu-O bonds and the simulations (dotted line) using the phases and amplitudes extracted from the Zn K edge EXAFS spectra. The k range is 2.6–10.6 Å^{-1}.

structure around the Cu atom. The indicated positions for Cu-Cu and Cu-Zn interactions are referenced according to bulk materials. The phases of these second peaks show a kink at ~4.3 $Å^{-1}$ which gives a separation of 0.36 Å. Interestingly, this value corresponds well to the separation between the Cu-Cu and Zn-Zn interactions in CuO and ZnO, respectively. The underlined reason for this agreement may be the similarity between Cu and Zn. The kink is strong for the Cu 7% film and very weak for the Cu 3% film for which the phase is similar to that of the Zn-Zn interaction in the ZnO host. Probably not by accident, the $\perp\varepsilon$ EXAFS oscillations of the Cu-O bond for the Cu 3% film can be fitted perfectly using the phase and amplitude extracted from the Zn *K* edge EXAFS for the Zn-O bond (the insert in Fig. 6 and the same S_0^2 assumed). The attempt to do the same using the parameters from bulk CuO is not successful; the S_0^2 value has to be increased by ~18% in order to have a decent simulation. It may be implicitly suggested that not only the Cu atoms substitute for the Zn ones in this sample but also that the Cu-O bonds have a property similar to that of the Zn-O bonds in the ZnO host. The Cu-O bond length such determined is 1.95 Å. The second peak belongs exclusively to the Cu-Zn interaction. The simulations for the Cu 7% film give less satisfactory results. This is likely caused by the coexistence of Cu-O bonds as part of clusters and as Cu_{Zn}. For the Cu 14% film, the first neighbor can be described fully by bulk CuO.

In order to extract the σ^2 value that is directly comparable to those obtained for the Zn *K* edge data presented in Sec. V, a FEFF8 simulation of the $\perp\varepsilon$ EXAFS data for the Cu 3%-doped film using a wurtzite $Cu_{Zn}O$ cluster with $S_0^2=0.9$ is carried out (dotted line in Fig. 6), from which $\sigma^2=0.0068$ $Å^2$. The third cumulant analysis of the Cu-O bond gives $R=1.95$ Å, being consistent with the result obtained above, and $\sigma^2=0.0076$ $Å^2$ with $C_3=-3.2\times10^{-4}$. Therefore, $[Cu_{Zn}O_4]$ is slightly more disordered than $[ZnO_4]$ in the ZnO host ($\sigma^2=0.0054-0.0060$ $Å^2$).

Based on the structures described above, it is now possible to understand the $L\rightarrow M$ feature and the downward shift of the 3*d* peak for these samples. In the Cu 3% film, the Cu_{Zn}-O distance is about equal to the Cu-O distance in bulk CuO. Based on the Brown-Shannon equation, this may suggest that the orbital overlapping in these bonds is comparable, resulting in the $L\rightarrow M$ feature to be located at similar energies. However, the transition is weaker (maybe, broader as well), relative to bulk CuO, which may be caused, e.g., by a *Franck-Condon* effect. Since a wurtzite $[Cu_{Zn}O_4]$ unit has a bonding configuration off sp^3, the increased *d* component in the bonding is thus expected, resulting in the 3*d* peak at a lower energy. For the Cu 14% film, the 3*d* peak moves to slightly higher energy (Fig. 5) but still differs from that of bulk CuO. This may indicate that the $[CuO_4]$ units in the cluster may not be as *planar* as the ones in bulk CuO.

Despite the complexity of the spectra, it is shown that Cu incorporation into the ZnO lattice takes place in O_2-prepared films. The Cu_{Zn}-O bond has a property similar to that of the Zn-O bond in the ZnO host. Thus, the $[Cu_{Zn}O_4]$ structure seems to be *blending* well with the ZnO host. With increasing doping level, more CuO clusters form.

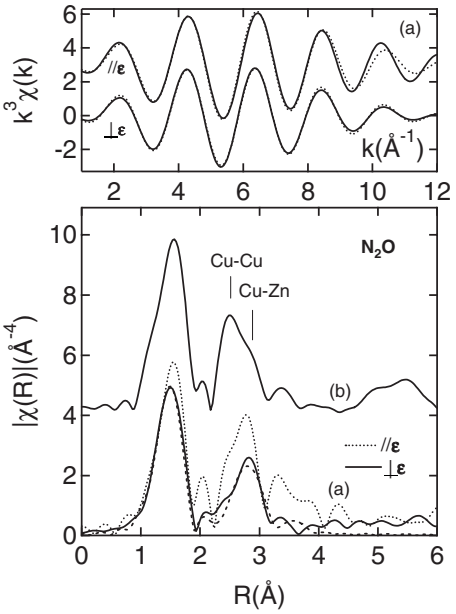

FIG. 7. Upper: Cu *K* edge EXAFS oscillations of the Cu-O bonds in the (a) Cu 1% doped film and the simulations using the phase and amplitude from the Cu-O bond in bulk CuO. Bottom: p-RDFs of the Cu-K edge EXAFS spectra for (a) Cu 1% and (b) Cu 7%. A FEFF8 simulation of the Cu 1% film using a $Cu_{Zn}O$ cluster is also shown (dashed line). The *k* range is 2.6–10.6 $Å^{-1}$.

B. Cu *K* edge data of the N_2O-prepared films

Similarly to the samples prepared in the O_2 environment, the copper occupation of the Zn site in the lattice (Cu_{Zn}) takes place in the N_2O-prepared films. With increasing doping level, more CuO clusters form as well. Even at a 1% copper doping, a clearly discernable amount of the Cu atoms are found to form in clusters. Figure 7 shows, in the lower panel, the p-RDFs for Cu 1% measured both at $\perp\varepsilon$ and $\|\varepsilon$ and for Cu 7% obtained at $\perp\varepsilon$. When compared to the data for O_2-prepared films in Fig. 6, it is found that for the same doping level these films tend to contain more CuO clusters. The simulation results of the Cu-O interaction in the Cu 1% film using the phase and amplitude extracted from bulk CuO are shown in the inset. The inferior fit quality for the $\|\varepsilon$ data is likely due to coexistence of Cu-O and Cu_{Zn}-O bonds.

Contrary to the case encountered for the O_2-prepared Cu 3% film, use of the parameters from the ZnO host does not yield satisfactory fit results for the $\perp\varepsilon$ data of the N_2O-prepared Cu 1% film until S_0^2 is reduced from 0.90 to ≤0.76 (the effect is inversed here), an indication that the many-body effect is prominent in this system. Also shown in Fig. 7 is the FEFF8 simulation result (dashed line) using a wurtzite $Cu_{Zn}O$ cluster with $S_0^2=0.76$, from which $R=1.925$ and $\sigma^2=0.0065$. The FEFF8 simulation of the Cu_{Zn}-O bond with C_3 included shows that $R=1.925$ Å and $\sigma^2=0.0075$ $Å^2$, respectively, with $C_3=-3.6\times10^{-4}$. Therefore, in this Cu 1% film, the Cu_{Zn}-O bond is *shorter* than the counterpart in the O_2-prepared films (1.95 Å), which represents a 12% increase in the bonding covalence. Although the disorder around the Cu_{Zn} atom is comparable to that found in the O_2-prepared film ($\sigma^2=0.0068-0.0076$ $Å^2$), it is consid-

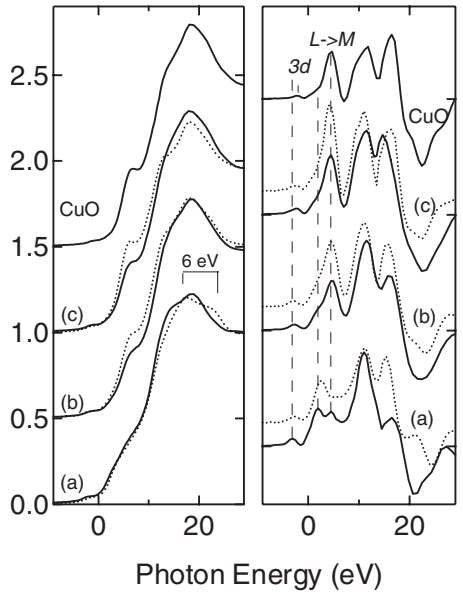

FIG. 8. Cu K edge XANES spectra and the first derivatives of N_2O-prepared films measured at two sample orientations: $\|\varepsilon$ (solid line) and $\perp\varepsilon$ (dotted line). (a) Cu 1%; (b) Cu 7%; and (c) Cu 10% compared to bulk CuO. The zero energy is set to the Cu K edge of metal.

erably larger than that around the Zn atom in its ZnO host ($\sigma^2=0.0026$ Å^2). The shoulder corresponding to the Cu-Cu interaction is more prominent in the $\|\varepsilon$ data. This indicates an in-plane orientation of the CuO clusters. For the Cu 7% film, $R_{\text{Cu-O}}=1.95$ Å, not surprisingly close to that of bulk CuO.

To illustrate the corresponding electronic structures in these films, Fig. 8 displays the Cu K edge XANES spectra in a way similar to that for the O_2-prepared films. *Unlike* the O_2-prepared films, a much larger polarization dependence of the XANES structures is seen here. Moreover, the density of states for the Cu 1% film extends to lower energies, a situation found for small CuO clusters in which strong covalent Cu-O bonds form, resulting in the downward shift of the $L\rightarrow M$ feature (Fig. 1). The first derivatives show more clearly an electronic structure *strikingly* different from the one for O_2-prepared films. There exists a *twin* $L\rightarrow M$ feature in the $\|\varepsilon$ data; one of which belongs to the CuO clusters ($\Delta E_{(L\text{-}M)\text{-}3d}=7.5$ eV) and the other is associated with the Cu_{Zn}-O bond in the ZnO lattice ($\Delta E_{(L\text{-}M)\text{-}3d}=5$ eV). The latter is a result of the shorter more covalent Cu_{Zn}-O bond (or 10% more covalent than Cu-O in bulk CuO). The cluster $L\rightarrow M$ feature is missing in the $\perp\varepsilon$ projection, indicating on the one hand that the CuO clusters consists of planner $[CuO_4]$ blocks which have an in-plane orientation, and on the other hand, the $\perp\varepsilon$ XANES should represent, for the most part, the electronic structure of the Cu_{Zn} atoms.

It is also noticed that for $\perp\varepsilon$, both the $3d$ peak and the $L\rightarrow M$ feature locates at slightly higher energies. Such a correlated shift shows the intrinsic relation between these two electronic states. The shift of the $\|\varepsilon$ $3d$ peak with doping level relates to the planer $[CuO_4]$ content.

Unlike in the O_2-prepared films, the Cu_{Zn}-O bond lengths in the N_2O-prepared films are shorter than the Zn-O bond length in the host lattice ($\Delta R\sim 0.04$ Å). Assuming a perfect 90° alignment of the $\hat{c}$ axis to the sample surface and a perfect tetrahedron for $[ZnO_4]$ or $[Cu_{Zn}O_4]$, the difference in the bond distance between Zn-O and Cu_{Zn}-O results in a 2% contraction of the tetrahedron height (R/R_0) along the $\hat{c}$-axis and a 6% contraction in the tetrahedron volume $[(R/R_0)^3]$. Assuming an even distribution of the Cu_{Zn} atoms in the host lattice, the $\hat{c}$-axis lattice constant will contract by $\sim$0.02% for the Cu 1% doping film, on average. It is more complicated to estimate the lattice changes for other samples. However, a general trend of contraction with increasing doping level may be expected given the preferred in-plane orientation of the CuO clusters in the N_2O-prepared films. Therefore, the x-ray-absorption measurements confirm the x-ray-diffraction data published in Ref. 5 for these samples, with enhanced microscopic details.

VII. DISCUSSIONS

From the study of films grown at a 10 cm t-s distance, we have demonstrated that the films containing only copper clusters are not ferromagnetic, regardless of the cluster sizes. From the study of films grown at an 8 cm t-s distance, we have demonstrated that the substitution of Cu^{2+} for Zn^{2+} is not the only imperative condition for ferromagnetism, wherein both the O_2-prepared and the N_2O-prepared films give evidence of such substitution, but only the films grown in N_2O are ferromagnetic. A close relation between the screening (final-state) effect due to the $L\rightarrow M$ charge transfer and the covalence (initial state) is firmly established for all the films.[18] The coherent variation in $3d$ and $L\rightarrow M$ features as well as S_0^2 with the bond property is uncovered. The following discussion will be focused only on the 8 cm t-s grown films.

Unlike the O_2-prepared films the N_2O-prepared films are ferromagnetic.[5] There are also clear differences between the electronic and atomic structures of the O_2-prepared films and the N_2O-prepared films. The most striking difference is that in the O_2-prepared films the Cu_{Zn} sites commensurate (blend) well with the host lattice, while in the N_2O-prepared films the Cu_{Zn} sites are distinctly different from the host lattice, both in terms of the physical dimension and chemical property of the Cu_{Zn}-O bonds. As shown in Secs. V and VI, for an ionic Zn-O bond in ZnO $S_0^2=0.90$, while for the more covalent Cu-O bond in CuO it is 0.76. The smaller S_0^2 value is resulted from the many-body (final-state) effect in the electron excitation process via the $L\rightarrow M$ charge transfer.[16] In addition to the comparable bond lengths, the fact that the Cu_{Zn}-O bond can be described by the Zn-O bond ($S_0^2=0.9$) in the host for the O_2-prepared Cu 3% film may reveal an explicitly ionic aspect for this Cu_{Zn}-O bond. In the N_2O-prepared films, the screening effect is stronger and the Cu_{Zn}-O interaction is covalent. We will argue that the covalent Cu_{Zn}-O bonds play an essential role in the establishment of the ferromagnetic ordering in these ZnO:Cu films.

Given the electronic and atomic structures in the O_2-prepared films, the copper doping should introduce neither n-type nor p-type carriers, which renders it difficult for any carrier-mediated processes to occur. Moreover, for an

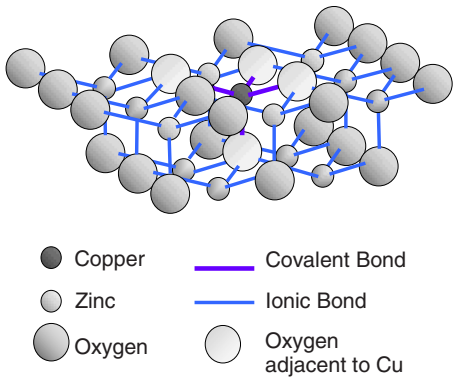

FIG. 9. (Color online) A cartoon depicting the effect of a covalent $[Cu_{Zn}O_4]$ structure in the wurtzite ZnO lattice.

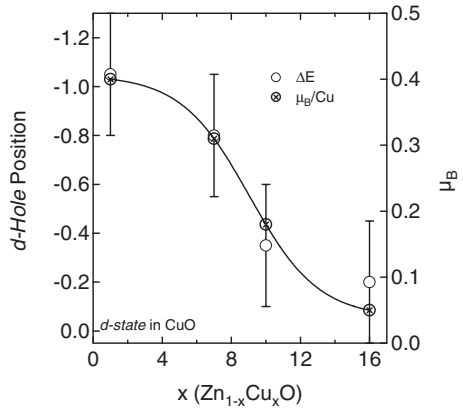

FIG. 10. The *d*-hole positions measured from the Cu *K* edge XANES spectra are plotted over the magnetic moments published in Ref. 5 as a function of the copper-doping concentration.

ionic oxide, the anion is at the zero-spin state, which should hardly participate in the magnetic coupling. The unpaired 3*d* electrons are pinned to a low-energy state by the electrical dipole field along the bonds, $\hat{e}_i$ $(=Q/\varepsilon R^2)$; $\Sigma\hat{e}_i \neq 0$ for a tetrahedron. As a result, the O_2-prepared films despite Cu^{2+}/Zn^{2+} substitution are only paramagnetic. Disorder in the lattice found in these films may arguably be disadvantageous to ferromagnetic ordering as well since it may compensate (remove degeneracy of) any holes in the valence band.

On the contrary, the ZnO host of the N_2O-prepared films showed a stronger wurtzite character. When comparing to the host $[ZnO_4]$ structure that has a smaller Debye-Waller factor, the disorder found around the Cu_{Zn} atom in these films appears to be excessive. The shorter covalent Cu_{Zn}-O bonds and the smaller $[Cu_{Zn}O_4]$ units appear to be incommensurate with the ionic host. Figure 9 is presented to illustrate the consequences of the covalent Cu_{Zn}-O bond in an ionic lattice. Due to the covalence the bonding electrons are itinerant within the Cu_{Zn}-O bond, which should induce an electron deficit in the neighboring Zn-O bonds and thus introduce holes in the valence band, a condition arguably favorable for the carrier-mediated ferromagnetism.[22] This implies that the Cu doping acts as an acceptor in these films (like Cu^{1+} doping), which introduces local moments, and holes residing in the host valence band with *p* character. The smaller $[Cu_{Zn}O_4]$ units will inevitably form compressed regions.

It may be interesting to view this from a different perspective. Since the energy position of the $L \rightarrow M$ feature is related to bonding covalence, the argument may be made that the lower the energy position is and the better the moment-carrying ions are screened locally. Using the relation $[1 + (E^{\text{film}}_{L\rightarrow M} - E_{Cu_2O})/(E^{\text{CuO}}_{L\rightarrow M} - E_{Cu_2O})]$, an effective charge of the Cu_{Zn} ion may be estimated to be 1.15, where $E=2$, 4.5, and 1.57 eV for the film, bulk CuO $L \rightarrow M$ peaks, and the absorption edge of bulk Cu_2O, respectively, referenced to the metal copper edge. In the formula, the unity is the charge of the Cu ion in Cu_2O. Therefore, this is the charge on the Cu_{Zn} ion that is seen by the "outside world," and the Cu substitution is purely a doping of the acceptor states. The ordered host lattice should maintain the highest possible degeneracy of the valence hole states.

The relatively larger disorder found around Cu_{Zn} may be due in part to a Jahn-Teller effect for a d^9 configuration.[23] This is clearly inconsistent with the calculation results on the distortion reported in Ref. 24. It may be even argued, in fact, that this disorder is essential for covalent bonds since the repulsion, especially in the basal plane, among the bonding electrons will be relieved. The repulsion may be significant when these electrons participate in spin exchange with the unpaired 3*d* moment. Therefore, the disorder may very well be intrinsic to the covalent bonds in these films. The Zn *K* edge results imply little oxygen defects in the films (see Sec. V).

Sudakar *et al.*[4] attributed the ferromagnetism to the planar nanoscale CuO inclusions in the ZnO:Cu thin films prepared by reactive magnetron sputtering. Our findings on the films containing only copper oxide clusters are inconsistent with this assertion (see Sec. IV). On the other hand, one of the structural results presented in this paper for ferromagnetic films is that even at the smallest doping level there is a small fraction of copper that forms in-plane oriented planar CuO clusters and that with increased doping level, the clusters dominate the system. Similar to the samples reported in Ref. 4, the magnetic moment per Cu atom in our samples decreases as the copper doping increases. Figure 10 displays the *d*-hole positions and the magnetic moments vs Cu concentration. A remarkable correlation is seen between these quantities. The interpretation of these data could be used to either negate or support the cluster argument raised in Ref. 4 if the detailed electronic and atomic structures were not available. As is firmly established in Sec. VI, the low-energy 3*d* state is related to the tetrahedrally coordinated Cu atoms on the Zn sites. Therefore, Fig. 10 elegantly demonstrates that the planar CuO clusters do not contribute (and in fact, is detrimental) to the observed ferromagnetism.

The results presented here provide solid experimental support to the theoretical work by Ye *et al.*,[24] which are confirmed very recently by Xiong *et al.*,[25] on a broad basis. We have shown eloquently that the substitution is a Cu^{2+} to a Zn^{2+} site, which will provide the necessary magnetic moments. However, such substitution alone is not sufficient for ferromagnetism, as demonstrated for the O_2-prepared films. The formation of the stronger covalent Cu_{Zn}-O bond, as predicted by Ye *et al.*,[24] is needed to establish an appropriate condition for ferromagnetic ordering to occur, as described in

the N_2O-prepared copper-doped films. Clearly, the Ruderman-Kittel-Kasuya-Yosida indirect exchange mechanism does not apply for these highly resistive films since it requires conduction electrons. The superexchange interaction used for oxidation-induced ferromagnetic coupling does not seem to be suitable for diluted samples described here either since it is a rather local mechanism.[26] In fact, the overall characteristic of the electronic and atomic structures of these films provides nearly all the necessary ingredients to understand the observed ferromagnetism based on the theoretical pictures for *p*-type DMS systems, such as $Ga_{1-x}Mn_xAs$,[22] carrier-mediated coupling.

VIII. CONCLUSION

We reported the local structures of a series of ZnO:Cu films grown by pulsed-laser ablation under various conditions. The results show that a film in which copper exists only as clusters is not ferromagnetic even for clusters as small as $[CuO_4]$. There is hardly any interaction between the clusters and the host lattice, which is essential for coupling to occur. In fact, the clustering is shown to be detrimental in the ferromagnetic films. It is also shown for O_2-prepared films that although the copper substitution of zinc in the ZnO lattice as the Cu^{2+} state provides necessary unpaired spins, it is not the only imperative factor for the ferromagnetism to occur in the ZnO:Cu films. When the formed $[Cu_{Zn}O_4]$ structures commensurate with the lattice in terms of both physical dimension and chemical properties, the copper doping does not introduce acceptor states, and no ferromagnetism is observed. For N_2O-prepared films where Cu_{Zn} occurs, the $[Cu_{Zn}O_4]$ structure is constructed with strong covalent Cu-O bonds. As a result the copper doping acts as an acceptor, introducing *p*-character holes in the valence band. The characteristic of the electronic and atomic structures of these films favors a ferromagnetic ordering mechanism via carrier-mediated spin alignments, as outlined in Ref. 22 for $Ga_{1-x}Mn_xAs$ systems.

ACKNOWLEDGMENTS

Work at Northwestern was supported by NSF (under its MRSEC program: Grant No. DMR-0076097), DARPA via Grant No. N00014-02-1-0887, and NASA via Award No. 521-0077-050A14/NCC2-1363. DND-CAT was supported by the E. I. DuPont de Nemours & Co., The Dow Chemical Co., the NSF under Grant No. DMR-9304725, and the State of Illinois under Grant No. IBHE HECA NWU 96. The APS was supported by the DOE under Contract No. W-31-109-Eng-38. We would also like to thank L.-H. Ye and A. J. Freeman for their helpful discussions.

*Author to whom correspondence should be addressed. q-ma@northwestern.edu

[1] D. Chakraborti, J. Narayan, and J. T. Prater, Appl. Phys. Lett. **90**, 062504 (2007).
[2] D. L. Hou, X. J. Ye, H. J. Meng, H. J. Zhou, X. L. Li, C. M. Zhen, and G. D. Tang, Appl. Phys. Lett. **90**, 142502 (2007).
[3] T. S. Herng, S. P. Lau, S. F. Yu, J. S. Chen, and K. S. Teng, J. Magn. Magn. Mater. **315**, 107 (2007).
[4] C. Sudakar, J. S. Thakur, G. Lawes, R. Naik, and V. M. Naik, Phys. Rev. B **75**, 054423 (2007).
[5] D. B. Buchholz, R. P. H. Chang, J. H. Song, and J. B. Ketterson, Appl. Phys. Lett. **87**, 082504 (2005).
[6] J. K. Furdyna, J. Appl. Phys. **53**, 7637 (1982).
[7] T. Hayashi, M. Tanaka, T. Nishinaga, H. Shimada, H. Tsuchiya, and Y. Otuka, J. Cryst. Growth **175-176**, 1063 (1997).
[8] S. J. Pearton, Y. D. Park, C. R. Abernathy, M. E. Overberg, G. T. Thaler, J. Kim, F. Ren, J. M. Zavada, and R. G. Wilson, Thin Solid Films **447-448**, 493 (2004).
[9] H. X. Liu, S. Y. Wu, R. K. Singh, L. Gu, D. J. Smith, N. Newman, N. R. Dilley, L. Montes, and M. B. Simmonds, Appl. Phys. Lett. **85**, 4076 (2004).
[10] S. J. Pearton, D. P. Norton, K. Ip, Y. W. Heo, and T. Steiner, J. Vac. Sci. Technol. B **22**, 932 (2004).
[11] S. J. Pearton, W. H. Heo, M. Ivill, D. P. Norton, and T. Steiner, Semicond. Sci. Technol. **19**, R59 (2004).
[12] A. Punnoose, H. Magnone, M. S. Seehra, and J. Bonevich, Phys. Rev. B **64**, 174420 (2001).
[13] T. S. Herng, S. P. Lau, S. F. Yu, H. Y. Yang, and X. H. Ji, J. Appl. Phys. **99**, 086101 (2006).
[14] C. Brouder, J. Phys.: Condens. Matter **2**, 701 (1990).
[15] D. E. Sayers, E. A. Stern, and F. W. Lytle, Phys. Rev. Lett. **27**, 1204 (1971).
[16] J. J. Rehr and R. C. Albers, Rev. Mod. Phys. **72**, 621 (2000).
[17] D. T. Jiang, E. D. Crozier, and B. Heinrich, Phys. Rev. B **44**, 6401 (1991).
[18] T. Miyanaga, H. Sakane, and I. Watanabe, Phys. Chem. Chem. Phys. **2**, 2361 (2000); G. Dalba, P. Fornasini, and F. Rocca, Phys. Rev. B **47**, 8502 (1993).
[19] S. E. Shadle, J. E. Penner-Hahm, H. J. Schugar, B. Hedman, K. O. Hodgson, and E. I. Solomon, J. Am. Chem. Soc. **115**, 767 (1993).
[20] I. D. Brown and R. D. Shannon, Acta Crystallogr., Sect. A: Cryst. Phys., Diffr., Theor. Gen. Crystallogr. **29**, 266 (1973).
[21] T. Mizoguchi, M. Kunisu, I. Tanaka, A. Nakamura, K. Matsunaga, T. Yamamoto, Y. Ikuhara, and W. Y. Ching, Microsc. Microanal. **10**, 92 (2004).
[22] A. H. MacDonald, P. Schiffer, and N. Samarth, Nature Mater. **4**, 195 (2005).
[23] D. Khomskii, in *Spin Electronics*, Lecture Notes in Physics, edited by M. Ziese and M. J. Thornton (Springer-Verlag, Berlin, 2001), pp. 89–116.
[24] L.-H. Ye, A. J. Freeman, and B. Delley, Phys. Rev. B **73**, 033203 (2006).
[25] Z. H. Xiong, S. Q. Shi, Q. X. Wan, and F. Y. Jiang, Phys. Scr., T **T129**, 358 (2007).
[26] K. Tono, A. Terasaki, T. Ohta, and T. Kondow, Phys. Rev. Lett. **90**, 133402 (2003).